ORIGINAL CONTRIBUTION

Effects of nano-fumed silica and carbonyl iron powder of different particle sizes on the rheological properties of shear thickening fluids

Fei Guo[1] · Zhedong Xu[1] · Jiming Gu[2]

Abstract

In this study, shear thickening fluid (STF) samples with different mass fractions were prepared by uniformly dispersing high-purity spherical silica powder in the polyethylene glycol (PEG) medium using the ball milling process. The influence of nano-particles on the shear and compression thickening effects of the STF dispersion system was investigated through the addition of fumed silica. Furthermore, the ball milled carbonyl iron powders (CIPs) with different particle sizes were dispersed uniformly in the STFs to prepare magnetorheological-STF (MR-STF) samples. The rheological properties of the developed STF and MR-STF samples were studied experimentally through a rheometer, and the results show that a lower temperature leads to a more obvious shear thickening effect of the STFs and that a smaller critical shear rate value promotes this effect. A higher content of silica powder also causes a more significant shear thickening effect of the STFs. Moreover, the addition of nano-fumed silica can significantly enhance the shear thickening effect, and the transition from continuous to discontinuous STFs can be realized by increasing the fumed silica mass fraction. Similarly, higher contents of silica powder and nano-fumed silica in the compression mode result in a more obvious thickening effect. In addition, the size of the CIP particles and the magnetic field strength directly affect the shear thickening effect of the MR-STFs. Specifically, under the same ferromagnetic particle mass fraction, the larger the CIP particles, the higher the applied magnetic induction intensity. Although a significant MR effect can be obtained, a certain inhibitory weakening effect is produced for the shear thickening behavior of the MR-STFs. Finally, considering the results in combination with the hydro-clustering and jamming theories, a mechanism was established to reveal the influence of different silica powder contents and nano-fumed silica fillings on the shear and compression thickening effects of STFs. Besides, a mechanism was proposed for the inhibition of the shear thickening effect of the MR-STFs by the ordered structures formed by CIP particles of different sizes in a magnetic field.

Keywords STF · Fumed silica · CIP · Particle size · Rheological properties · Mechanism

Introduction

Shear thickening fluids (STFs) are a new type of intelligent material usually consisting of stable submicron spherical particles uniformly dispersed in a suspension system comprising ethylene glycol, polyethylene glycol (PEG), and other dispersion media. Under normal conditions, STF materials behave as fluids. Once they experience high-speed impact or compression, their viscosity rises sharply, and they

digest the external force, showing obvious characteristics of non-Newtonian fluids. After the removal of the external force, the materials return to their initial fluid state, which manifests their strong ability to absorb impact. The shear thickening effect of STFs is sensitive to the shear strain rate and, therefore, does not require an applied magnetic or electric field for operation, as is the case for magnetorheological (MR) and electrorheological (ER) materials. Devices developed using these materials are passive; therefore, STFs have promising applications in structural vibration control in engineering [1–3], human protection [4–6], and other fields.

STFs have attracted worldwide attention due to their unique mechanical properties, and the research hotspots mainly focus on the factors influencing the properties of STF materials and the shear thickening mechanism. Researchers have found that the material properties [7–10], mass fraction

✉ Fei Guo
  hhulcygf@163.com

1 School of Civil Engineering and Architecture, Anhui Polytechnic University, Wuhu 241000, China

2 School of Management Science and Engineering, Anhui University of Technology, Ma'anshan 243002, China

[11, 12], and size and shape [13, 14] of the dispersed particles and the type of dispersion media [15–18] are the key factors influencing the shear thickening effect of STFs. Furthermore, the pH value of the suspension system [19] and external influences such as the temperature [20–24], loading conditions [25], and various types of additives [26–29] have a significant influence in this regard, where suitable additives can remarkably enhance the effect.

Targeting the working mechanism of the shear thickening of STFs, researchers have proposed theories such as the order–disorder transition (ODT) [30, 31], hydro-clustering [32, 33], and jamming [34] theories. At its core, Hoffman's ODT theory states that at a relatively low shear rate, the STF suspension system fails to generate the thickening effect due to the ordered layered structure of the internal particles, but as the shear rate increases, the lamellar structure of the particles is destroyed, resulting in a sharp rise in the STF viscosity. According to the hydro-clustering theory by Wagner and Brady, the shear thickening effect of STFs arises because particles overcome intermolecular forces and Brownian motion under fluid dynamics and subsequently form particle clusters. Using the small-angle light scattering (SALS) technique [35, 36], Crawford found that large particles formed during the shear thickening phenomenon are 2–3 µm in size and can be considered clusters resulting from the accumulation of small particles. The jamming theory mainly states that dispersed particles at higher mass fractions are subject to relatively weak Brownian motion and have more contact with each other. When the shear rate reaches a certain critical value, flow jamming occurs inside the STF, followed by a sharp increase in viscosity. In addition, existing research results have revealed that over a wide shear rate range, an STF usually undergoes three stages of transformation [37]—shear thinning, shear thickening, and shear thinning—as shown in Fig. 1. Specifically, η_0 denotes the initial viscosity, $(\dot{\gamma}_c, \eta_c)$ denotes the critical point marking the change from shear thinning to shear thickening, and $(\dot{\gamma}_{max}, \eta_{max})$ denotes the critical point indicating the change from shear thickening to shear thinning. In terms of the shear thickening effect of STFs, one should mainly note the location of the critical point $(\dot{\gamma}_c, \eta_c)$ and the increase in the magnitude of the viscosity to the maximum value at $\dot{\gamma}_{max}, \eta_{max}$.

Considering the similarity between an STF and an MR fluid (MRF) as a dispersion system composed of particles and a carrier liquid, Zhang et al. [38] first dispersed ferromagnetic particles in an STF in a certain proportion and synthesized a novel MR-STF dispersion system displaying an MR effect. After investigating the effects of different mass fractions of ferromagnetic particles on the shear thickening effect of an MR-STF, Sokolovski et al. [39] found that a higher content of ferromagnetic particles contributes to a better MR effect, while the shear thickening effect of the MR-STF is inhibited to a certain extent. Yang
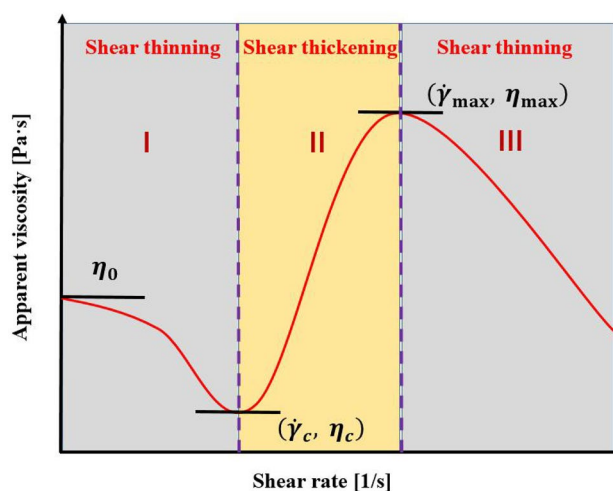

Fig. 1 Viscosity characteristic zones of the three STF stages [37]

et al. [40] developed and tested a linear damper filled with an MR-STF with a ferromagnetic particle content of either 20% or 80%—the results showed that the former presents better MR and shear thickening effects and that the latter is similar to traditional MR dampers in performance. In another study, Liu et al. [41] developed an MR-STF with ferromagnetic particle mass fractions in the range of 10–70% and tested automobile shock absorbers with this MR-STF and a commercial MRF containing the same fractions. The test results indicated that a better damping force can be obtained by filling the automobile shock absorbers with the self-developed MR-STF.

At present, several studies continue to focus on STFs or MRFs alone, while multifunctional MR-STFs based on their combination are seldom researched. Thus, the development of novel materials integrating two or more functions becomes an important direction for future development in the smart material sector. In this paper, high-purity spherical silica powder was used as the dispersed phase and PEG as the dispersion medium to prepare STFs with different dispersed phase mass fractions via the ball milling process. The effects of temperature and two sizes particle grade formed by adding fumed silica on the position of the critical point and the shear and compression thickening effects of the STFs were explored. Moreover, through the addition of soft magnetic particles of different sizes, the effects of ferromagnetic particle size and magnetic field intensity on the shear thickening of MR-STFs with the same ferromagnetic particle mass fractions were investigated. Based on the experimental results, models were then constructed to reveal the working mechanisms underlying (1) the effects of different silica powder contents and the addition of fumed silica on the thickening of the STFs and (2) the impact of ferromagnetic particle

size and magnetic field intensity on the shear thickening of the MR-STFs.

Materials and methods

Experimental materials

The main materials used in the experiments were silica powder (average particle size: 500 nm, Suzhou Nanodispersions Co., Ltd.) as the dispersed-phase particles, PEG-400 and absolute ethanol (Sinopharm Chemical Reagent Co., Ltd.) as the dispersion media, M-5 fumed silica (average primary particle size: 12 nm, Sinopharm Chemical Reagent Co., Ltd.) as the nano-additive, and carbonyl iron powder (CIP) particles (average particle size: 3.5 μm, Fe content: 98.1%, specific saturation magnetization: 177.1A·m^2/kg, Jiangsu Tianyi Ultra-Fine Metal Powder Co., Ltd.).

Preparation process

Herein, the STF suspension system was prepared through ball milling and dispersion in a ball mill, as shown in Fig. 2a. The specific procedures are described as follows:

1. High-purity silica powder and PEG-400 were weighed in a certain proportion, mixed, and stirred in an electric mixer for 15 min. Subsequently, a certain mass fraction of M-5 fumed silica was added to the mixed suspension system of selected samples, which was stirred for another 15 min in the electric mixer.
2. The uniformly stirred solid–liquid suspension system was then placed into a mill pot, followed by the addition of large and small steel balls (with diameters of 12 and 6 mm, respectively) in the numerical ratio of 1:5.
3. The mill pot was securely placed in an SHQM double planetary ball mill, with a rotational speed of 100–150 m/min, followed by a 30-min comprehensive grinding process to ensure that the dispersed-phase particles were uniformly dispersed in the suspension system.
4. After grinding, the mixed sample was vacuumized to remove air bubbles and obtain an STF sample with complete and uniform dispersion.

To explore the effects of soft magnetic particles on the rheological properties of STFs, CIP particles of different sizes were also generated by the ball milling process, and four dispersed-phase types of MR-STF samples were prepared. The procedure is illustrated in Fig. 2b and described as follows:
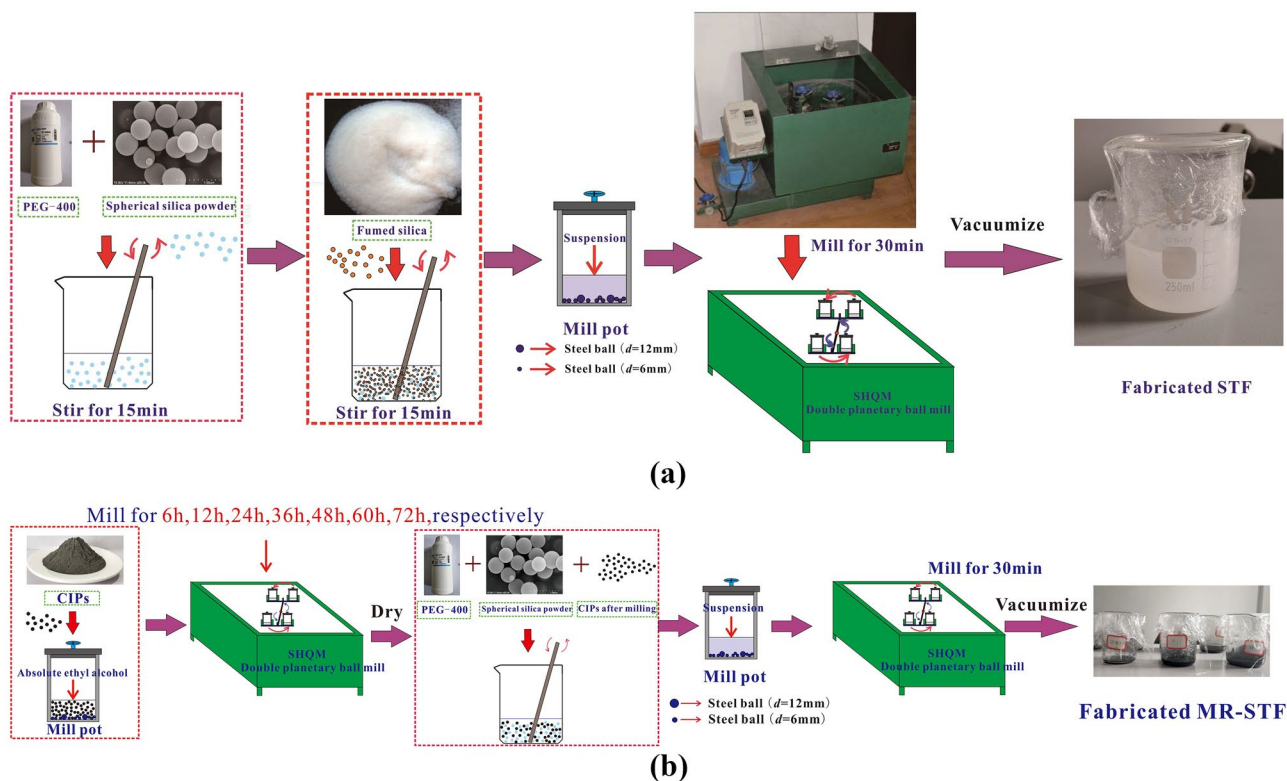

Fig. 2 Preparation process of **a** STF samples and **b** MR-STF samples with different CIP particle sizes

1. CIP particles (initial particle size: 3.5 μm) and absolute ethanol (dispersion medium) were weighed in proportion and placed in a mill pot. Large and small steel balls with the same diameters and numerical ratio as those in the STF sample preparation were then added to the mill pot.

2. The mill pot was securely placed in the SHQM double planetary ball mill operating at a rotational speed of 200–250 m/min. Subsequently, ball milling was performed for 6, 12, 24, 36, 48, 60, and 72 h, respectively, for the different samples.

3. The resultant ground CIP samples were then dried in a high-temperature drying oven to prepare different sizes of CIP particles.

4. High-purity silica powder, CIP particles of different sizes, and PEG-400 (dispersion medium) were weighed in proportion, mixed, and stirred in an electric mixer for 15 min. The soft magnetic particles selected herein were the 3.5 μm CIP particles (not ball milled) and those ball milled for 6, 24, and 60 h.

5. Each uniformly stirred solid–liquid suspension system was transferred to a mill pot, followed by the addition of large and small steel balls with the same diameters and numerical ratio as in the previous procedures. The mill pots were securely placed in the SHQM double planetary ball mill, operating at a rotational speed of 100–150 m/min, followed by a 30 min comprehensive grinding process to ensure uniform dispersion of the particles in the suspension system.

6. After grinding, the mixed samples were vacuumized to remove air bubbles and yield MR-STF samples with full and uniform dispersion.

In these experiments, 10 groups of STF and 4 groups of MR-STF samples were prepared, respectively, the main components and particle mass fractions of which are provided in Table 1. The mass fraction of the dispersed-phase CIP particles in the MR-STF samples was 5%.

Property characterization

To measure the particle size distribution of the CIPs after ball milling, a testing device based on the D8 Advance X-ray diffractometer was assembled, as shown in Fig. 3a, c. According to the scanning electron micrograph of the CIP particles in Fig. 3b, the ferromagnetic particles displayed relatively obvious spherical characteristics. In Fig. 3d, the particle size distribution of the CIP ball milled for 24 h reveals a normal distribution at a particle size of 600 nm. The particle size distribution of CIPs ball milled for different times is shown in Fig. 3e; one can easily note that with the increase in the ball milling time, the size of the ferromagnetic particles decreases from the initial 3.5 μm to 300 nm after 72 h of ball milling. Here, the particle sizes of 1350 and 360 nm corresponding to 6 and 60 h of ball milling, respectively, were selected.

The rheological properties of the prepared STF and MR-STF samples were tested and analyzed with the MCR302 rotational rheometer system, composed of an MCR302 rheometer (host), a magnetic field excitation module (magnetic field device), and a temperature control device (DC-2006 low temperature constant temperature bath, temperature range − 20–100°), as shown in Fig. 4. In these experiments, the rotational speed of the PP20 parallel plate rotor was adjusted to gradually increase the shear rate from 0 to 50 s^{-1}. The correlation between the apparent viscosity

Table 1 Main components and mass fractions of dispersed-phase particles in STF and MR-STF samples

| Sample no.	Silica powder	PEG-400	M-5 (fumed silica)	CIP	Mass fraction (dispersed-phase particles)
STF-1	31.85 g	20.00 g	\	\	61.4%
STF-2	36.00 g	20.00 g	\	\	64.3%
STF-3	40.87 g	20.00 g	\	\	67.1%
STF-4	43.64 g	20.00 g	\	\	68.6%
STF-5	46.67 g	20.00 g	\	\	70%
STF-6	50.00 g	20.00 g	\	\	71.4%
STF-6-A	49.40 g	20.00 g	0.6 g	\	71.4%, including M-5–0.86%
STF-6-B	49.00 g	20.00 g	1 g	\	71.4%, including M-5–1.43%
STF-6-C	48.50 g	20.00 g	1.5 g	\	71.4%, including M-5–2.14%
STF-7	53.68 g	20.00 g	\	\	72.9%
MR-STF-0 h	50.00 g	20.00 g	\	3.68 g	72.9%, including CIP-5%
MR-STF-6 h	50.00 g	20.00 g	\	3.68 g	72.9%, including CIP-5%
MR-STF-24 h	50.00 g	20.00 g	\	3.68 g	72.9%, including CIP-5%
MR-STF-60 h	50.00 g	20.00 g	\	3.68 g	72.9%, including CIP-5%
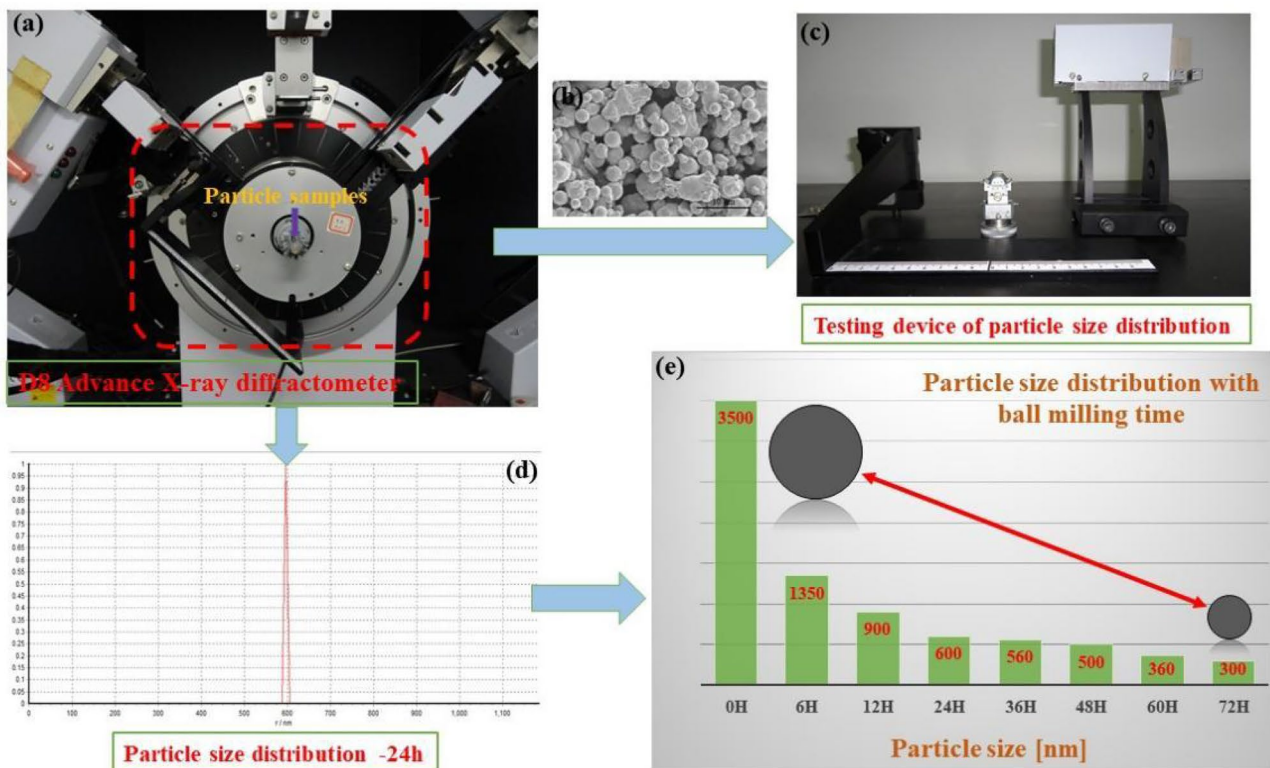
Fig. 3 **a** D8 Advance X-ray diffractometer, **b** scanning electron micrograph of a CIP sample, **c** testing device of particle size distribution, **d** particle size distribution of the CIP after ball milling for 24 h, and **e** change law of particle size distribution of CIPs with ball milling time

and the shear rate of the STFs was subsequently analyzed to characterize the shear thickening effect of the STFs. Moreover, the MCR302 rotational rheometer system was used to perform a vertical static compression test to characterize the thickening effect of the STFs in the compression mode. In such a system, the magnetic field excitation module can generate a continuously adjustable magnetic field intensity, thus allowing one to test the MR effects of materials such as MRFs. In this paper, the rheological properties of MR-STF samples under the action of different magnetic field intensities were mainly characterized.

Results and discussion

Shear rheological properties

Experimental results and analysis

In the experiment, the different testing temperatures could be maintained through circulating water controlled by the DC-2006 low temperature constant temperature bath. The flow curves of the apparent viscosity and shear stress of sample STF-7 against the shear rate at different temperatures

are plotted in Fig. 5. PEG-400, as the carrier material of the STFs, is sensitive to temperature to a certain extent; the lower the temperature, the more obvious the shear thickening effect of the STF. The results mainly show that the larger the initial viscosity η_0, the smaller the values of the shear rate at the critical points, $\dot{\gamma}_c$ and $\dot{\gamma}_{max}$, and the larger the peak viscosity value η_{max}. In STF-7, a peak viscosity of 885 Pa·s and a maximum shear stress of 30 kPa were obtained at 16 ℃.

To further quantify the influence of temperature on the shear thickening effect of STF-7, the ratio η_{max}/η_c was used as a key index to measure the shear thickening effect. The changes in the critical shear rate values ($\dot{\gamma}_c$ and $\dot{\gamma}_{max}$) and the shear thickening effect η_{max}/η_c of STF-7 with temperature are shown in Fig. 6. It is evident that, on the one hand, the critical shear rate values increase with the rise in temperature. For example, at 16 °C, STF-7 exhibits shear thickening behavior when the shear rate is 2.07 s^{-1}, while the viscosity peak is reached at a shear rate of 22.6 s^{-1} as the sample starts to enter the shear-thinning zone. At 35.2 °C, it does not enter the shear-thickening zone or reach the peak viscosity within the test area before the shear rates $\dot{\gamma}_c$ and $\dot{\gamma}_{max}$ reach 8.35 and 50 s^{-1}, respectively. On the other hand, as the temperature increases, the shear thickening effect of STF-7

Fig. 4 MCR302 rotational rheometer system
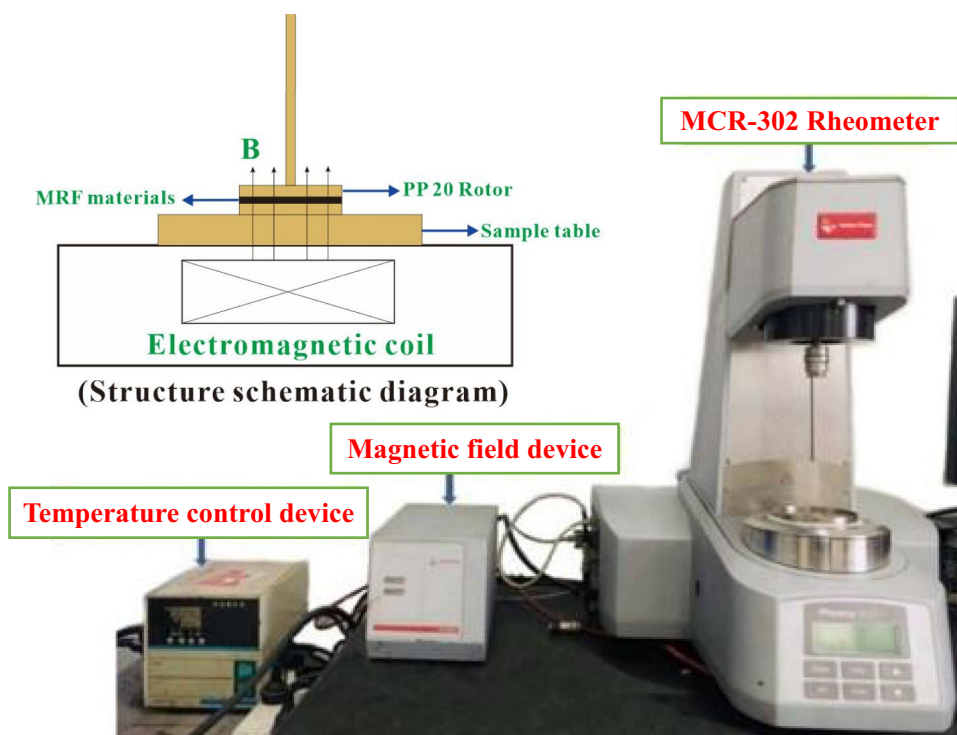
gradually decreases from 19.45 to 7.97. Hence, temperature is a crucial factor influencing the shear thickening effect and critical points of STF materials. At higher temperatures, the Brownian motion of the particles is more obvious, and the intermolecular forces can effectively overcome the variation in the spatial structure due to the changing shear rate. In contrast, at lower temperatures, the Brownian motion is weaker, and it is difficult for the intermolecular forces to overcome the variation in the spatial structure triggered by the shear rate. Thus, the shear thickening effect becomes more obvious at lower temperatures, and the critical transition phenomena occur at earlier stages.

Figure 7 shows the flow curves of the apparent viscosity and shear stress of the STF samples (with different silica powder mass fractions) against the shear rate at a constant temperature. In the shear rate range of 0–50 s^{-1}, almost no shear thickening effect is observed in samples STF-1 and STF-2, containing silica powder mass fractions of 61.4 and 64.3%, respectively. As the silica powder mass fraction increases, the shear thickening effect of the STFs becomes
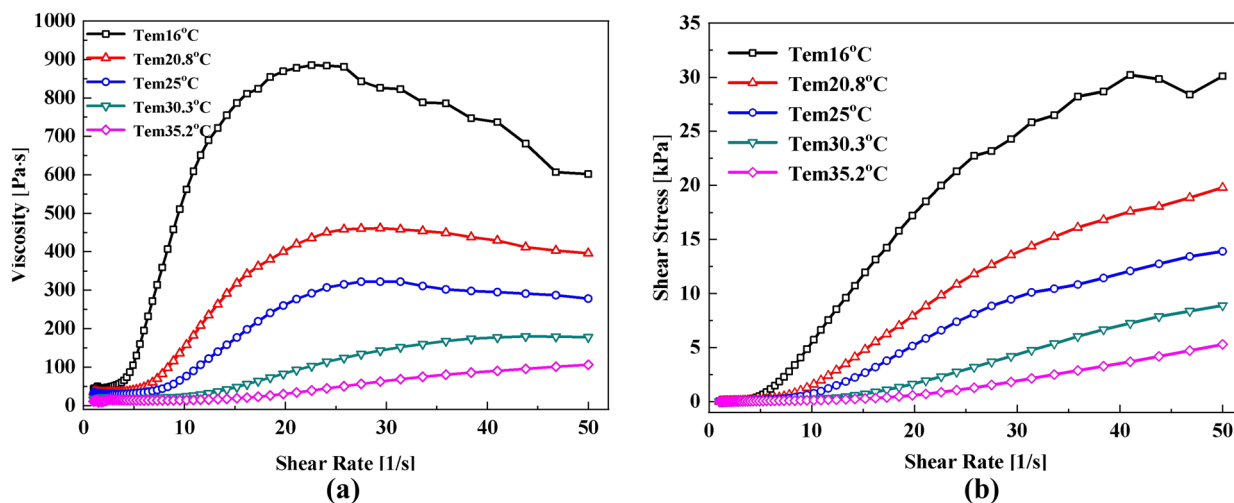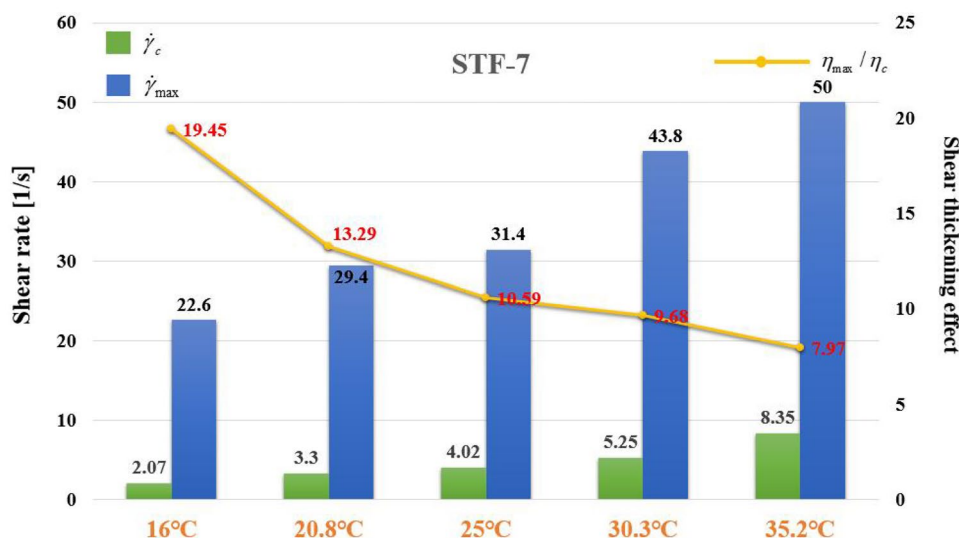

Fig. 5 Influence of temperature on the shear thickening effect of STF-7: **a** correlation between viscosity and shear rate and **b** correlation between shear stress and shear rate

Fig. 6 Shear thickening effect and change law of the critical shear rate with temperature for STF-7

more obvious. At a particle mass fraction of 72.9% in STF-7, the apparent viscosity and shear stress experience a sharp rise with the increase in the shear rate, and the maximum viscosity and shear stress reach 406 Pa·s and 17.7 kPa, respectively. Moreover, except for STF-7, the STF samples all reach their peak viscosity at 50 s^{-1} within the testing interval between 0 and 50 s^{-1}, and further shear thinning might be observed over a wider shear rate range.

Figure 8 depicts the flow curves of the apparent viscosity and shear stress against the shear rate for STF samples with different mass fractions of M-5 fumed silica at a constant temperature. One can observe that at a shear rate of 50 s^{-1}, samples STF-6 and STF-6-A, B, and C (with the added M-5) all reach the peak viscosity values within the

test range. Figure 8 indicates that the addition of a small amount of fumed silica can significantly improve the shear thickening effect of STFs. At a constant silica particle mass fraction, samples STF-6-A, B, and C (with M-5 contents of 0.86, 1.43, and 2.14%, respectively) display increases of 90.1, 146.1, and 277.1 Pa·s in the maximum apparent viscosity and increases of 4.6, 7.4, and 13.9 kPa in the maximum shear stress, respectively, compared with STF-6 (with no added M-5).

Shear thickening mechanism

The parameters of different STF types can be fitted to the power law equation $\tau = K\dot{\gamma}^{a}$, and the obtained non-Newtonian
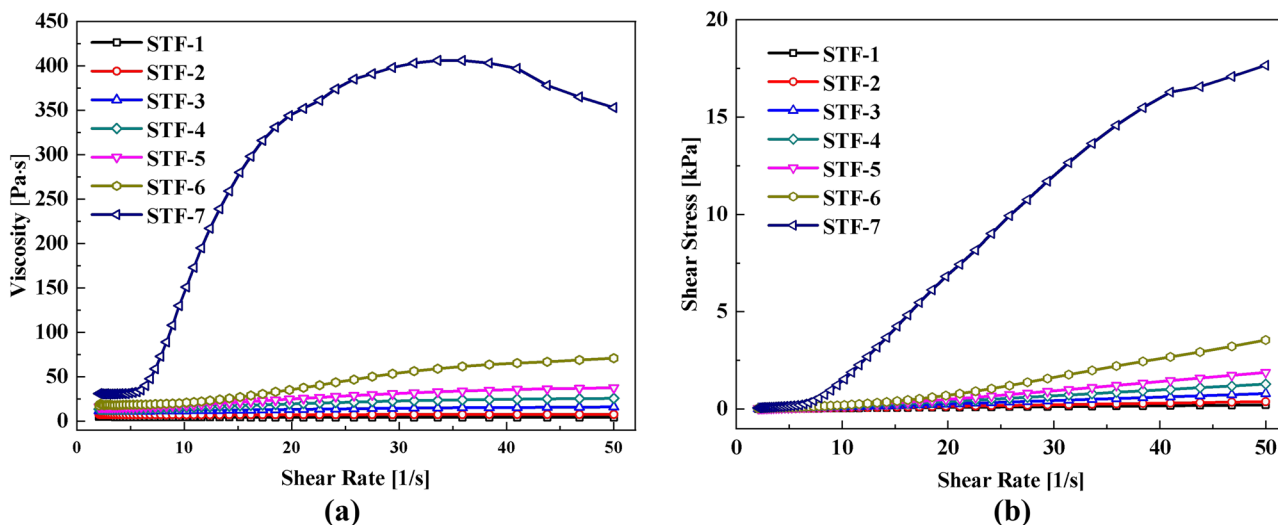

Fig. 7 Influence of different silica powder mass fractions on the shear thickening effect of STFs at a constant temperature of 23 °C: **a** correlation between viscosity and shear rate and **b** correlation between shear stress and shear rate
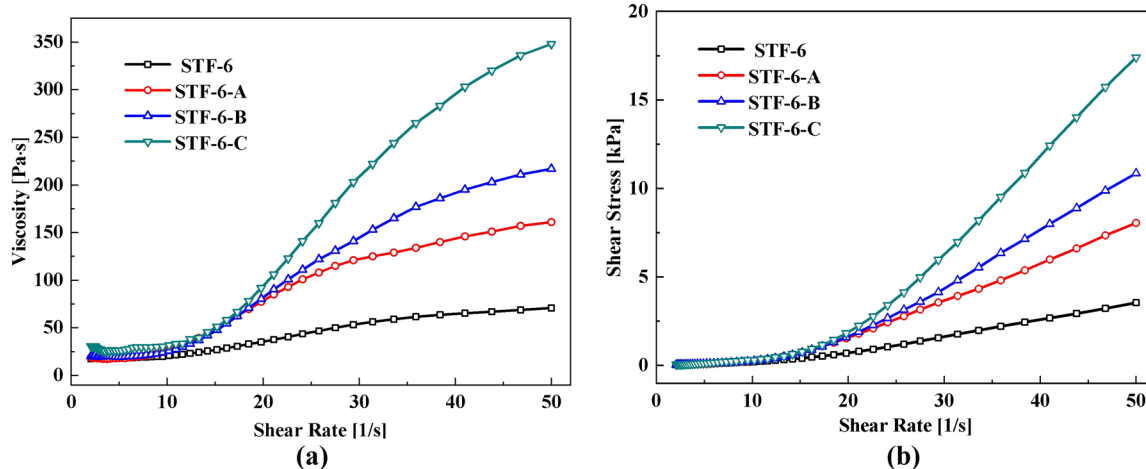
Fig. 8 Influence of M-5 fumed silica on the shear thickening effect of STFs at a constant temperature of 23 °C: **a** correlation between viscosity and shear rate and **b** correlation between shear stress and shear rate

coefficient a can be applied to quantitatively distinguish the STF types [13]. In terms of STFs, a is usually larger than 1, and larger a values lead to more obvious non-Newtonian behavior. Moreover, $1 < a < 2$ corresponds to continuous STFs, while $a > 2$ corresponds to discontinuous STFs. Through the fitting procedure, all the STF samples in this study were classified, as shown in Fig. 9a. At a low silica powder mass fraction, for example, STF-1 and STF-2, the a value is close to 1, and the STFs approximate a Newtonian fluid. With the increasing silica powder mass fraction, the non-Newtonian characteristics of the STFs become more obvious. Specifically, STF-3, STF-4, STF-5, STF-6, and STF-6-A, the a values of which are between 1 and 2, are continuous STFs. STF-7, with a silica powder mass fraction of 72.9% and an a value greater than 2, belongs to the

discontinuous STF group. The transition from continuous to discontinuous STFs can be achieved by adjusting the M-5 fumed silica content. For instance, when the mass fraction of the added M-5 reaches 1.43 and 2.14% in STF-6-B and STF-6-C, respectively, the a values of these STFs become greater than 2, indicating the transitioning of these two samples to discontinuous STFs.

Similarly, for samples STF-3 to STF-6, which display an observable shear thickening effect, as the silica powder mass fraction increases from 67.1 to 71.4%, the critical shear rate $\dot{\gamma}_c$ gradually decreases, as shown in Fig. 9b. Specifically, the $\dot{\gamma}_c$ values, stimulated by the shear thickening, decrease from 8.92 to 3.52 s^{-1}, and when the silica powder mass fraction reaches 72.9%, $\dot{\gamma}_c$ continues to decrease to 2.89 s^{-1}. The $\dot{\gamma}_c$ values also gradually decrease with increases in the mass
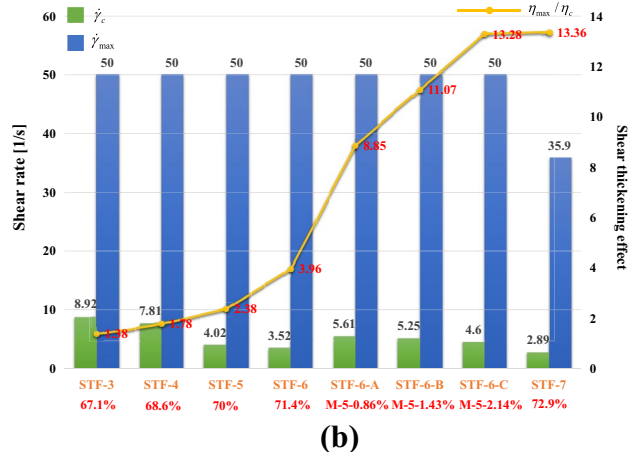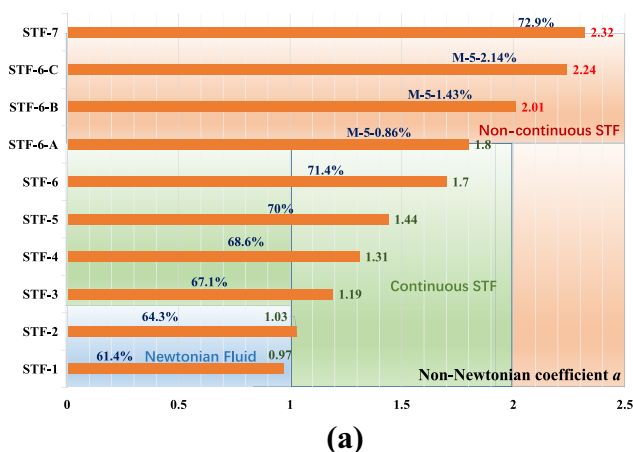

Fig. 9 **a** Classification of continuous and discontinuous STF types and their non-Newtonian coefficients a and **b** the shear thickening effect of STFs with different mass fractions of silica powder and M-5 fumed silica and the change law of the critical shear rates.
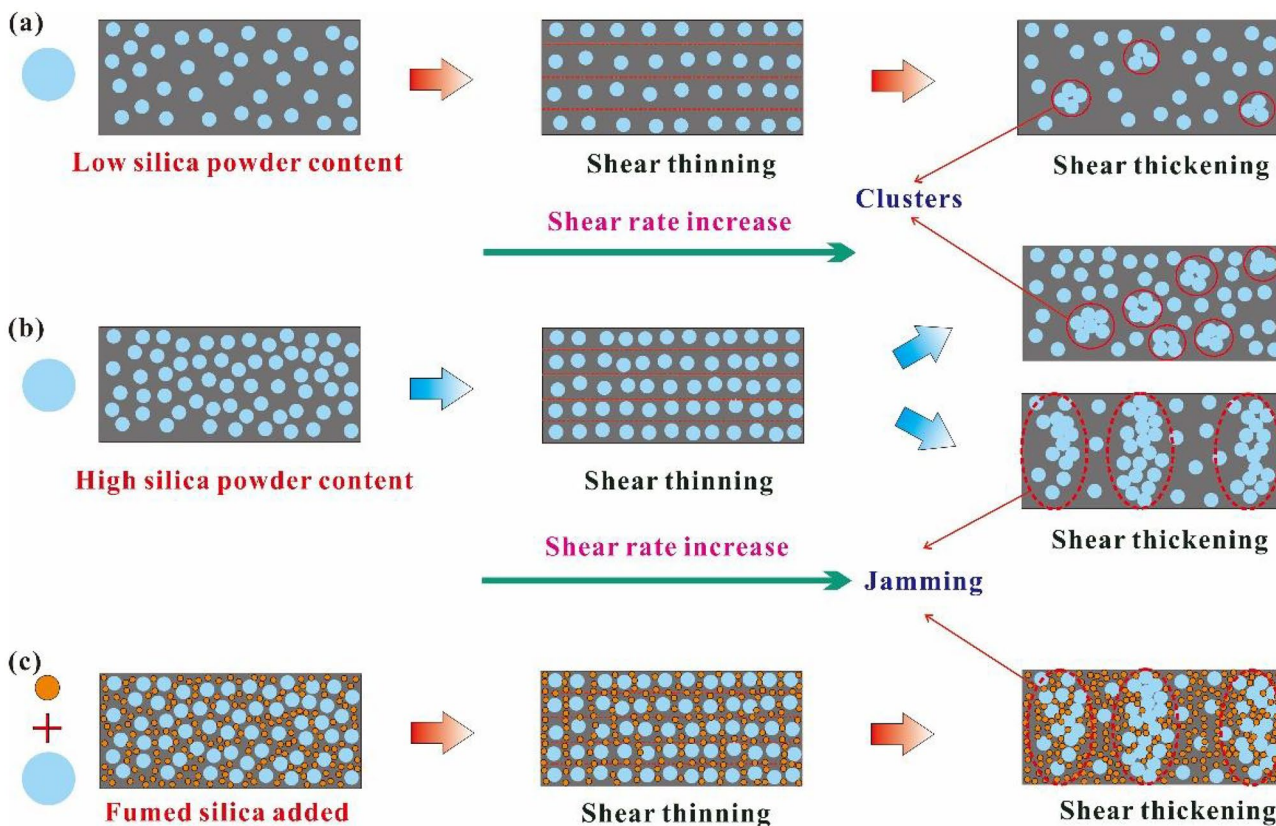
Fig. 10 Shear thickening mechanism of STFs with **a** low and **b** high silica powder mass fractions and with **c** the addition of fumed silica

fraction of the M-5 fumed silica; for STF-6-C, with an M-5 mass fraction of 2.14%, $\dot{\gamma}_c$ is 4.6 s^{-1}. When the silica powder mass fraction rises from 67.1 to 72.9%, the shear thickening effect, as measured by $\eta_{\max}/\eta_c$, increases substantially from 1.38 to 13.36. Similarly, as the mass fraction of M-5 increases from STF-6 (with no M-5) to STF-6-C, the shear thickening effect increases significantly from 3.96 to 13.28.

To better describe the shear thickening mechanisms of STFs with different silica powder mass fractions and the influence of fumed silica in this regard, a theoretical mechanism was proposed herein (Fig. 10). At a low silica powder content (Fig. 10a), the silica powder is uniformly dispersed in PEG-400 in the initial state. When the shear rate is very low, the disturbed equilibrium of the dispersion system can quickly return to the initial state under the action of Brownian motion and intermolecular forces, with the system showing a low and stable viscosity. With the gradual increase in the shear rate, the stress generated between the dispersed particles becomes greater than the forces between them. In this case, the dispersion system fails to completely overcome the changes in the system's spatial structure due to external influences. Thus, the particles form a layered structure under the action of fluid dynamics, resulting in shear thinning. As the shear rate further rises to the critical shear rate $\dot{\gamma}_c$, the

fluid force becomes evidently larger than the intermolecular forces between the particles and the Brownian motion, contributing to the formation of relatively unstable functional groups, that is, clusters. Subsequently, the viscosity grows
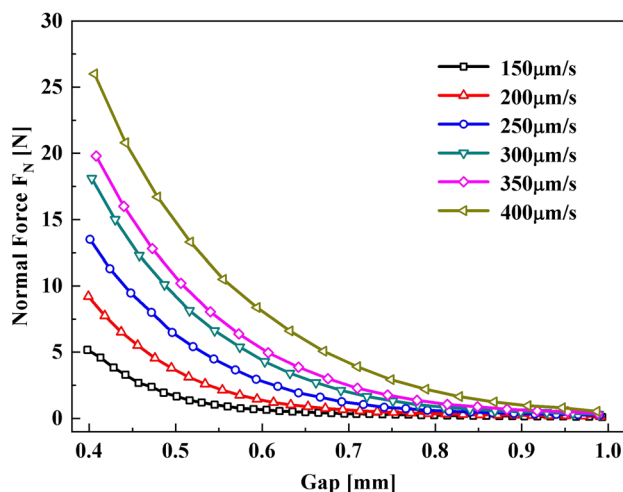

Fig. 11 Compression rheological properties of sample STF-7 at different compression rates in a constant temperature environment of 23 °C

significantly, ultimately leading to shear thickening. At a high silica powder content (Fig. 10b), because of the instability of clusters, the fluid force between the clusters further accumulates and leads to local jamming. Under the application of shear forces, the jamming gradually expands and spreads, completely preventing the flow of the suspension system. In other words, the shear force triggers the jamming, as manifested at the macroscopic level by a sharp increase in viscosity. For instance, when the particle mass fraction reaches 72.9%, the viscosity of STF-7 changes across orders of magnitude, with the sample possibly experiencing a "liquid–solid" transition. Regarding the addition of fumed silica to the STF samples (Fig. 10c), due to the large difference between the particle sizes of silica powder and fumed silica, the latter can effectively fill the gaps between the clusters formed by the silica powder particles. Thus, these clusters become denser, the jamming is more obvious, and the shear thickening effect is effectively enhanced.

Compression rheological properties

Experimental results and analysis

In this study, the compression thickening effect was measured based on the magnitude of the normal force generated when the STFs were subjected to vertical compression at the corresponding plate spacing. Figure 11 depicts the normal force–spacing curves of STF-7 at different compression rates in a constant temperature environment, with the initial plate spacing set at 1 mm. As shown in Fig. 11, the STF sample also presents a thickening or hardening effect when it is under a loading of positive effect, witnessing a

more prominent thickening effect and larger normal forces with increases in the compression rate. At a comparatively low compression rate (150 μm/s, for instance), the STF sample gradually generates a normal force only when the plates have been compressed to a spacing of approximately 0.65 mm rather than generating it immediately. A higher compression rate gives rise to a larger spacing for the generation of the normal force; this spacing approaches 1 mm when the compression rate reaches 400 μm/s.

Figures 12a, b depict the normal force–spacing curves of the STFs with different silica powder mass fractions and those with different fumed silica contents at the compression rate of 450 μm/s and under a constant temperature environment, with the initial plate spacing set to 2 mm. The thickening effect of the STFs is more apparent at a higher silica powder mass fraction. The plate spacing at which the samples start to generate a normal force is approximately 1.1 mm for STF-7, with a particle mass fraction of 72.9%, but decreases as the particle mass fraction drops. The addition of fumed silica, however, does not alter the plate spacing at which the normal forces of the samples start to emerge. Furthermore, though a normal force can be generated at a plate spacing of approximately 1.0 mm under the aforesaid two circumstances, the addition of fumed silica can significantly amplify the normal force of the STF samples as effectively as it increases the shear thickening effect. This means that the addition of fumed silica can effectively improve the compression thickening effect of the STFs, leading to a more apparent thickening effect at a higher fumed silica content.
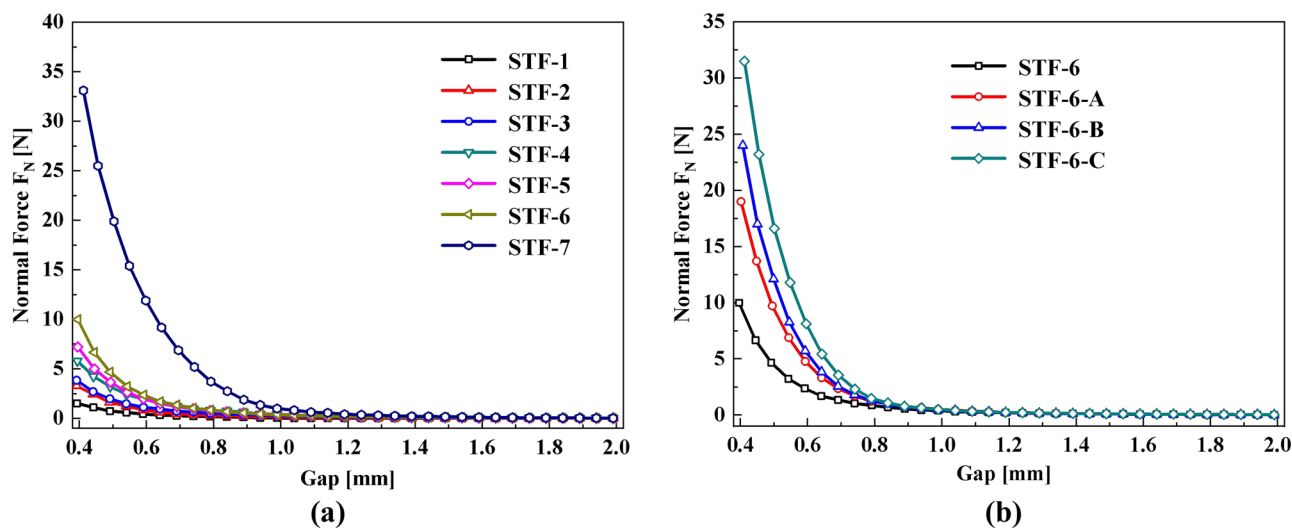

Fig. 12 Compression rheological properties of STF samples with different **a** silica powder and **b** fumed silica contents at a compression rate of 450 μm/s and a constant temperature of 23 ℃

Compression thickening mechanism

The thickening mechanism of the STFs with different silica powder mass fractions and fumed silica contents under compression is presented in Fig. 13. The silica powder is evenly dispersed in PEG-400 at the initial stage. As the compression starts, the vertical space of the dispersion system is gradually compressed under the action of the external force due to a gradual reduction in the plate spacing, leading to the spreading of the silica powder particles under the acting force of fluid dynamics. At a lower silica powder mass fraction (Fig. 13a), the comparatively smaller number of particles gradually gather into clusters under the action of fluid dynamics. Jamming might occur locally as the compression continues. Given the small number of particles, a normal force can be generated only when the vertical space has been compressed to a certain extent. At a higher silica powder mass fraction (Fig. 13b), however, due to the greater number of particles, the motion of the particles is more pronounced under the action of fluid dynamics as the vertical space is compressed, making it easier for them to cluster. Consequently, jamming occurs and can even escalate into complete blockades with no particle flow, substantially enhancing the normal force as a result. This explains why a normal force can be generated earlier at a larger plate spacing in the case of a higher silica powder content. The impact of the addition of fumed silica is reflected more in compensating for

the spacing between the clusters formed by the silica powder particles, which enhances the compactness and, thus, increases the magnitude of the normal force (Fig. 13c). In the entire dispersion system, however, the particle mass fractions remain constant; the difference lies only in the reduction in the amount of silica powder and its replacement by fumed silica. As a result, the plate spacing for the generation of the normal force remains essentially the same. Furthermore, the value of the compression rate serves as a determinant of how rapidly the vertical space is reduced. A larger compression rate implies greater fluid dynamics that render a higher possibility of shattering the intermolecular forces between and Brownian motion of the silica powder particles and consequently promoting their clustering in a shorter time and the generation of a normal force from the subsequent jamming.

MR-STF rheological properties

Experimental results and analysis

In this study, CIP particles ball milled for different durations were evenly dispersed in STFs to explore the influence of different sizes of ferromagnetic particles on the shear thickening effect of STFs. CIP, a common filling material for MR materials, such as MRFs and MR elastomers (MREs), can generate an MR effect in a magnetic field for adaptation to
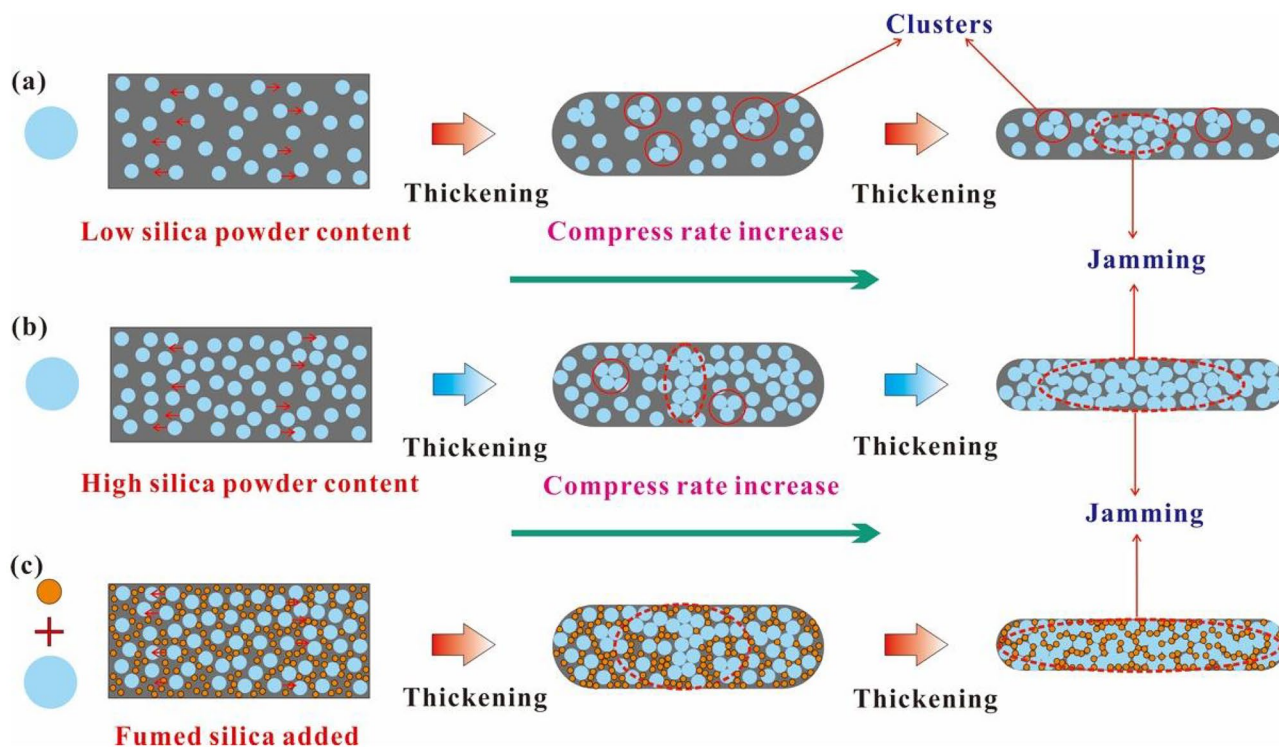

Fig. 13 Compression thickening mechanism of STFs with **a** low and **b** high silica powder mass fractions and with **c** the addition of fumed silica

Fig. 14 Changes in the viscosity of the MR-STFs with the magnetic field and shear rate and change laws for the MR effect ($\eta_{M0.45}/\eta_{M0}$, red two-dimensional bars), shear thickening effect ($\eta_{c\text{-max}}/\eta_c$), and degree of shear thinning (η_0/η_c): **a** MR-STF-60 h filled with 360-nm CIP particles, **b** MR-STF-24 h filled with 600-nm CIP particles, **c** MR-STF-6 h filled with 1.35-µm CIP particles, and **d** MR-STF-0 h filled with 3.5-µm CIP particles
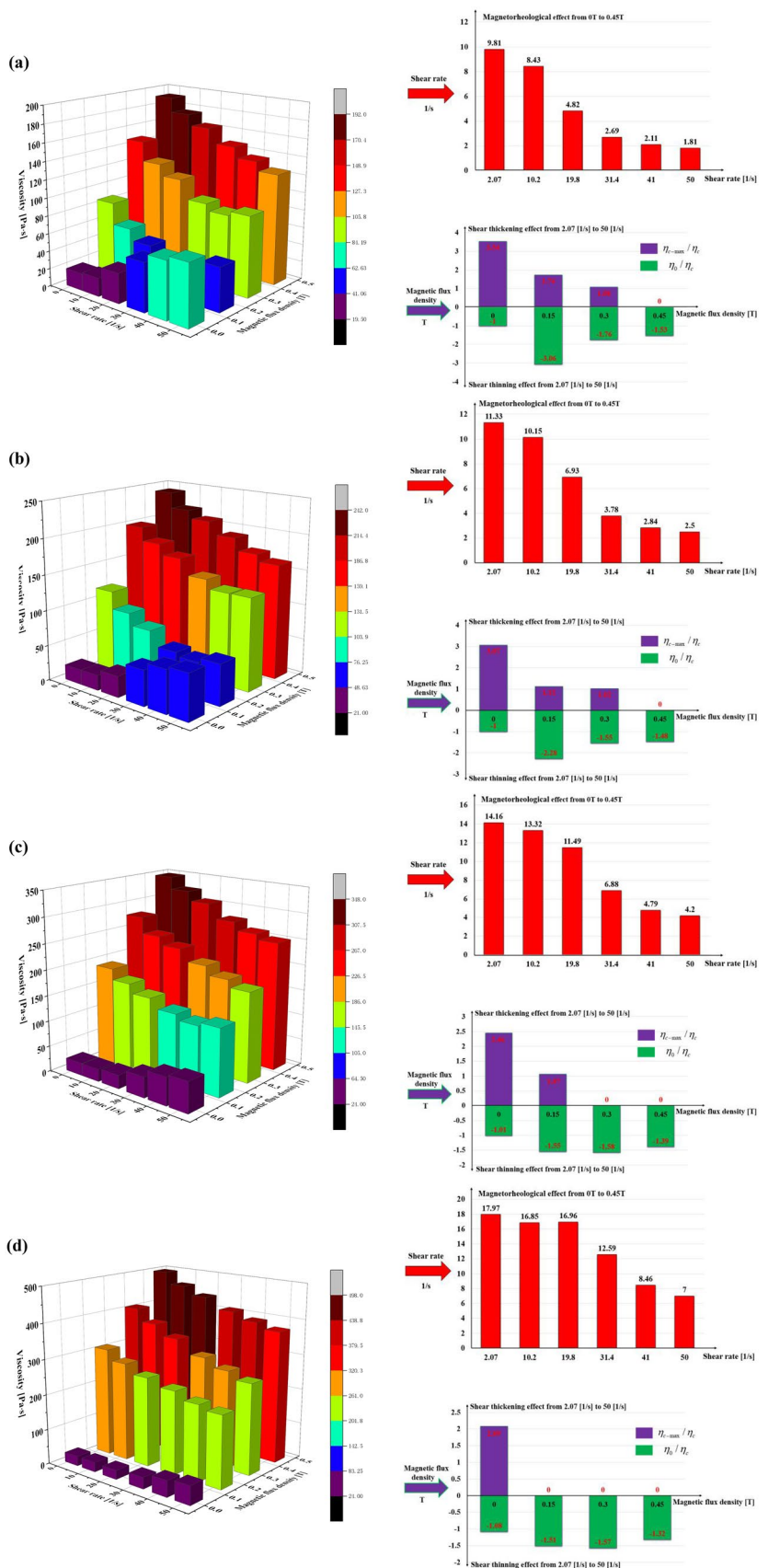
excitation from external environments. Therefore, its application enjoys a bright prospect in the field of semi-active vibration control. The addition of soft magnetic particles of CIP to STFs leads to a new type of MR-STF that possesses a dual regulatory mechanism and that displays both the shear thickening and the MR effects under the actions of the external excitation rate and magnetic field. As concluded in relevant studies, the mass fraction of CIP particles has a notably significant impact on MR-STFs. A higher CIP content is associated with an apparent MR effect but a comparatively low shear thickening effect; in other words, MR-STFs under such conditions can be regarded as equivalent to MRFs in effectiveness. At a low CIP content, however, the material manifests a better shear thickening effect in a weaker magnetic field environment. The impact of different CIP particle sizes on the shear thickening effect of STFs was explored as the focus of this study. Since using high CIP mass fractions was not suitable, the mass fractions of the CIPs with different particle sizes were all set to a constant value of 5%.

The CIPs—including one sample that was not ball milled (3.5 μm) and samples ball milled for 6 h (1.35 μm), 24 h (600 nm), and 60 h (360 nm)—were added to STFs with a silica powder mass fraction of 71.4%. The silica powder particle size was 500 nm; in comparison, the largest CIP particle size was approximately seven times larger, while the sizes of the nanoscale CIP particles were close to that of the silica powder particles. Figure 14 presents the rheological properties of the four MR-STF samples under the combined actions of the excitation rate and magnetic field, where the loaded magnetic induction intensity ranged from 0 to 0.45 T while the loaded shear rate was between 2.07 and 50 s^{-1}. Under the condition of identical shear rates, a higher magnetic induction intensity indicates a higher viscosity of the MR-STF sample in each group. As one can note from Fig. 14a–d, the viscosity of the MR-STFs rises as the CIP particle size increases. According to Fig. 14d, at a CIP particle size of 3.5 μm and a shear rate of 2.07 s^{-1}, the viscosity approaches 500 Pa·s when the applied magnetic induction intensity reaches 0.45 T, showing an almost twofold increase in viscosity compared to MR-STF-60 h under the same loading conditions. To better quantify the MR effect of the MR-STFs, the ratio of the viscosity at a magnetic induction intensity of 0.45 T to the viscosity in the absence of a magnetic field, $\eta_{M0.45}/\eta_{M0}$, was used as a measurement indicator. One can observe that the MR effect of the MR-STFs gradually drops as the shear rate continuously rises, with a more apparent MR effect at a larger ferromagnetic particle size. In Fig. 14d, the MR effect of MR-STF-0 h drops from 17.97 to 7 as the shear rate increases from 2.07 to 50 s^{-1}. In comparison, the MR effect in MR-STF-60 h in Fig. 14a decreases from 9.81 to 1.81 under the same conditions. Therefore, one can conclude that a larger CIP particle size gives rise to a

higher magnetic induction intensity and a more apparent MR effect of the MR-STFs. However, increases in the shear rate inhibit the MR effect to some degree.

Furthermore, the MR-STF samples in each group present a shear thickening effect to some degree under the condition of zero magnetic field; that is, the viscosity rises as the shear rate increases. When the applied magnetic induction intensity is maintained at a relatively low level of 0.15 T, MR-STF-6 h, filled with 1.35-μm CIP particles (Fig. 14c); MR-STF-24 h, filled with 600-nm CIP particles (Fig. 14b); and MR-STF-60 h, filled with 360-nm CIP particles (Fig. 14a) all exhibit shear thinning initially and a shear thickening effect after the critical shear rate is reached. In Fig. 14d, MR-STF-0 h, filled with the largest ferromagnetic particles, exhibits shear thinning behavior and the absence of the critical point of shear thickening throughout the entire observation range of the shear rate. When the magnetic induction intensity reaches 0.3 T, only MR-STF-24 h and MR-STF-60 h show initial shear thinning and subsequent shear thickening, while MR-STF-0 h and MR-STF-6 h, both filled with micron-scale CIP particles, experience only shear thinning over the entire observation range of the shear rate. When the magnetic induction intensity rises to 0.45 T, all the MR-STF samples show shear thinning only, and no shear thickening is observed. Likewise, under identical conditions of the magnetic induction intensity, the ratio $\eta_{c\text{-max}}/\eta_c$ was regarded as indicative of the shear thickening effect of the MR-STFs and is displayed above the x-axis and marked in the form of a positive number. $\eta_{c\text{-max}}$ represents the peak value of the viscosity after the critical shear rate has been reached. The ratio of the initial viscosity to that at the critical shear rate (η_0/η_c) was used as a measurement indicator of the degree of shear thinning and is displayed below the x-axis and marked as a negative number. One can note that the shear thickening effect of the MR-STFs gradually decreases as the magnetic induction intensity increases, with a weaker shear thickening effect in the case of a larger ferromagnetic particle size. In Fig. 14a, the shear thickening effect of MR-STF-60 h gradually decreases from 3.54 to 1.74, 1.08, and 0 as the magnetic induction intensity increases from 0 T to 0.15, 0.3, and 0.45 T, respectively. In comparison, the shear thickening effect of MR-STF-24 h in Fig. 14b gradually decreases from 3.07 to 1.12, 1.02, and 0 under the same conditions. Therefore, one can conclude that a larger CIP particle size is associated with a higher magnetic induction intensity and that they both inhibit the shear thickening effect of MR-STFs to some degree.

In addition, within the shear rate range of 2.07–50 s^{-1}, the MR-STF samples in each group show a nearly identical degree of shear thinning (approximately 1) in the absence of a magnetic field, indicating that the addition of CIP particles cannot affect the rheological properties of MR-STFs when no magnetic field is applied. However, as the size of

Fig. 15 Rheological mechanism of MR-STFs under the action of a magnetic field: **a** CIPs with small particle size, **b** CIPs with large particle size, and **c** the possible structures formed by silica particles and CIPs with different particle sizes
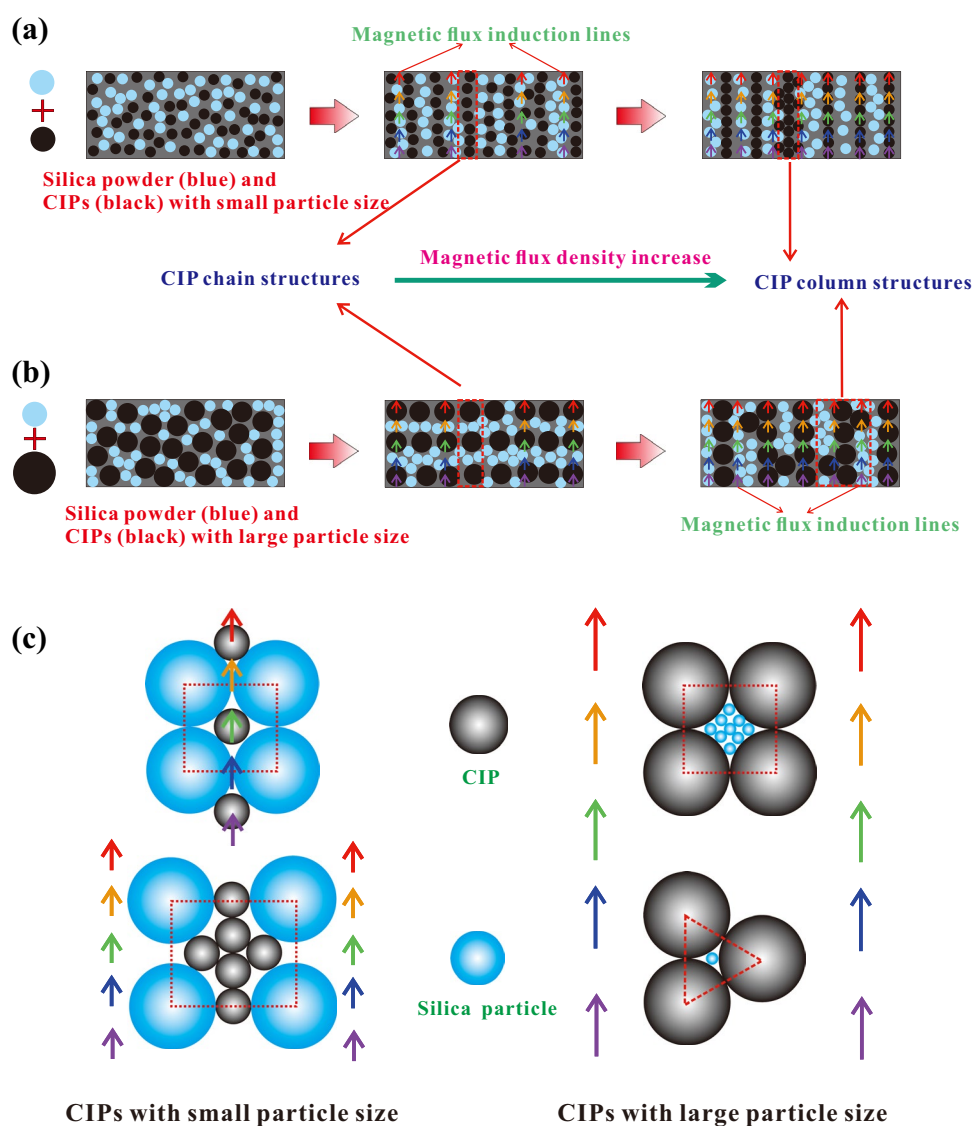
the CIP particles in the MR-STFs increases, the samples present a weaker degree of shear thinning overall. As shown in Fig. 14c, d, the micron-scale CIP particles exhibit a degree of shear thinning not exceeding 2 in all the MR-STF samples. The MR-STF samples in each group experience a decreasing degree of shear thinning as the magnetic induction intensity increases after the application of a magnetic field.

MR-STF rheological mechanism

MR-STFs offer both sensitivity to the shear rate and an MR effect under the combined excitation of a shear rate and a magnetic field. In other words, their viscosity and shear stress can be controlled for particular purposes by adjusting the applied shear rate and magnetic field intensity. The shear thickening mechanism of STFs has been discussed earlier. Figure 15 mainly depicts the working mechanism of MR-STFs under the action of a magnetic field based

on the assumption that the CIP particles in this model all possess spherical characteristics. According to Fig. 15a, b, the CIP and silica powder particles of different sizes were evenly dispersed in the PEG-400 medium in the absence of a magnetic field. According to relevant theories of magnetic dipoles [42], CIP particles in MR-STFs generate a magnetic interaction force between themselves after a magnetic field is applied, allowing the ferromagnetic particles to align and form an ordered chain structure along the direction of the magnetic flux induction line. Furthermore, a larger ferromagnetic particle size leads to a smaller plate spacing, giving rise to more prominent MR properties. As the magnetic induction intensity rises, the magnetic force between CIP particles gradually climbs to narrow the spacing between the ferromagnetic particles and bind them more tightly. Consequently, columns and other ordered structures might form to enhance the MR effect of MR-STFs.

As shown in Fig. 15a, b, as the CIP particles gradually move along the direction of the magnetic flux induction line to form ordered chain or column structures from an evenly dispersed disordered structure under the action of a magnetic field, collisions and friction occur between the CIP and silica powder particles due to the significant density gap between them, causing the latter to move into the limited structural space between various chain structures formed by the former. When the shear rate is loaded, the liquidity of the dispersion medium drops due to the obstruction of the ordered structures of the ferromagnetic particles and the space limitations. Consequently, the silica powder particles are forced into a spatial structure similar to the ordered structures of the ferromagnetic particles within a restricted area, thus facilitating the ordered development of the entire dispersion system and causing shear thinning as a result. However, when the particle size of the CIPs is similar to or smaller than that of the silica powder, the ferromagnetic particles form a chain structure with a comparatively large particle spacing under the condition of a weaker magnetic induction intensity, while the silica powder particles gradually gather and cluster after overcoming intermolecular forces and Brownian motion under the action of fluid dynamics (Fig. 15c), further enhancing the thickening effect to some extent. The gradual increase in the magnetic induction intensity leads to and reinforces the binding between the ferromagnetic particles, accompanied by the further gathering of the parallel chains of the particles to form column structures. However, the clustering of the silica powder particles is difficult due to the spatial structure limitations, adding to the difficulty of generating a thickening effect. MR-STF-60 h and MR-STF-24 h, for instance, contain CIP particles only 360 and 600 nm in size, respectively, but were able to generate a shear thickening effect when the magnetic induction intensity was maintained at 0.15 and 0.3 T. Nevertheless, no thickening was observed when the magnetic induction intensity rose to 0.45 T, explaining the inhibitory and weakening effect of magnetic induction intensity on the shear thickening effect of MR-STFs. Moreover, when the CIP particles are much larger than the silica powder particles, the magnetic interaction force of the former rises under the action of the magnetic induction intensity. As a result, the silica powder faces a larger possibility of being blocked in the micro spaces formed by the gathering of CIP particles (Fig. 15c). As the magnetic induction intensity rises, it becomes almost impossible for the silica powder particles to flow and gather under the action of fluid dynamics, making thickening impossible. In MR-STF-0 h, for instance, the 3.5-μm ferromagnetic particles are seven times larger than the silica powder particles. Under such circumstances, no shear thickening occurs when the magnetic induction intensity increases from a low to a high level, which explains why a larger ferromagnetic particle size inhibits the shear thickening effect of MR-STFs more significantly.

Conclusion

In this study, STF and MR-STF samples were prepared through the ball milling dispersion method. The rheological properties were investigated and the following conclusions were reached.

1. STFs are typical examples of materials with temperature-dependent rheological properties. Specifically, the shear thickening effect of STF-7 rose as the temperature dropped, mainly reflected in a decreasing critical shear rate and an increasing ratio of the maximum to the critical viscosity (η_{max}/η_c) under such circumstances. This is mainly attributed to the fact that a higher temperature leads to a more pronounced Brownian motion of the particles, which helps overcome the changes in the spatial structure with the application of shearing deformations.

2. The contents of the dispersed particles and nano-fumed silica effectively have a positive impact on the thickening effect, as reflected in the dispersion of the STFs in the investigations of shear and compressive rheology. A higher content of dispersion particles increases their possibility of clustering under the action of fluid dynamics, leading to subsequent jamming once their flow is blocked. Moreover, because of the large difference in particle size between the nano-fumed silica and the silica powder, the former can effectively fill the gaps between the clusters of accumulated silica powder particles, thus tightening the structure of such clusters and subsequently effectively improving the viscosity and shear stress of the STFs. STFs can be shifted from continuous ($a < 1$) to discontinuous ($a > 2$) by altering their nano-fumed silica content.

3. Both a larger CIP particle size and a higher applied magnetic field intensity inhibit and weaken the shear thickening effect of MR-STFs. CIP particles can quickly form into oriented ordered structures, such as chains or columns, under the action of a magnetic field. Due to a comparatively large difference in particle density, the silica powder particles become blocked in a limited structural space and suffer from restricted movement. At a higher magnetic field intensity, because ferromagnetic particles with a larger particle size are bound to each other more tightly, the restrictions on the silica powder particles are more apparent. Therefore, generating a shear thickening effect under such circumstances is difficult.

Data availability Thedata that support the findings of this study are available on request from thecorresponding author, upon reasonable request.

Declarations

Competing interests The authors declare no competing interests.

References

1. Lin K, Zhou AN, Liu HJ et al (2020) Shear thickening fluid damper and its application to vibration mitigation of stay cable. Structures 26:214–223
2. Guo YC, Wei YP, Zhou JL et al (2019) Impact and usage of the shear thickening fluid (STF) material in damping vibration of bolted flange joints. Smart Mater Struct 28:095005
3. Lim J, Kim SW (2020) Enhanced damping characteristics of carbon fiber reinforced polymer–based shear thickening fluid hybrid composite structures. J Intell Mater Syst Struct 31(20):2291–2303
4. Zhang JS, Wang Y, Deng HX et al (2022) A high anti-impact STF/Ecoflex composite structure with a sensing capacity for wearable design. Compos B 233:109656
5. Zhang JS, Wang Y, Zhou JY et al (2021) Intralayer interfacial sliding effect on the anti-impact performance of STF/Kevlar composite fabric. Compos A 145:106401
6. Yuan F, Liu S, Zhou JY et al (2020) A smart Kevlar-based triboelectric nanogenerator with enhanced anti-impact and self-powered sensing properties. Smart Mater Struct 29:125007
7. James NM, Han ED, de la Cruz RAL et al (2018) Interparticle hydrogen bonding can elicit shear jamming in dense suspensions. Nat Mater 17(11):965–970
8. Gamonpilas C, Morris JF, Denn MM (2016) Shear and normal stress measurements in non-Brownian monodisperse and bidisperse suspensions. J Rheol 60(2):289–296
9. Ye F, Zhu W, Jiang WQ et al (2013) Influence of surfactants on shear-thickening behavior in concentrated polymer dispersions. J Nanopart Res 15(12):2122
10. Liu M, Chen S, Wang S et al (2017) PVP immobilized SiO2 nanospheres for high-performance shear thickening fluid. J Nanopart Res 19(7):234
11. Zhao MM, Zhang JQ, Liu YL et al (2022) Rheological characteristics analysis of shear thickening fluids based on response surface methodology. Mater Res Express 9(2):025701
12. Mostafizur RM, Aziz ARA, Saidur R et al (2014) Effect of temperature and volume fraction on rheology of methanol based nanofluids. Int J Heat Mass Transf 77:765–769
13. Jiang WF, Xuan SH, Gong XL (2015) The role of shear in the transition from continuous shear thickening to discontinuous shear thickening. Appl Phys Lett 106(15):151902
14. Jiang WF, Peng GJ, Ma Y et al (2017) Measuring the mechanical responses of a jammed discontinuous shear-thickening fluid. Appl Phys Lett 111(20):201906

15. Qin JB, Zhang GC, Ma ZL et al (2016) Effects of ionic structures on shear thickening fluids composed of ionic liquids and silica nanoparticles. RSC Adv 6(85):81913–81923
16. Qin JB, Zhang GC, Shi XT (2016) Viscoelasticity of shear thickening fluid based on silica nanoparticles dispersing in 1-butyl-3-methylimidizolium tetrafluoroborate. J Dispersion Sci Technol 37(11):1599–1606
17. Li W, Xiong DS, Zhao XD et al (2016) Dynamic stab resistance of ultra-high molecular weight polyethylene fabric impregnated with shear thickening fluid. Mater Des 102:162–167
18. Shan L, Tian Y, Meng YG et al (2015) Influences of medium and temperature on the shear thickening behavior of nano fumed silica colloids. Acta Physica Sinica 64(6):068301
19. Chen Q, Zhu W, Ye F et al (2014) pH effects on shear thickening behaviors of polystyrene-ethylacrylate colloidal dispersions. Mater Res Express 1(1):015303
20. Wei MH, Sun L, Zhang CW et al (2019) Shear-thickening performance of suspensions of mixed ceria and silica nanoparticles. J Mater Sci 54(1):346–355
21. Sun L, Lv YR, Wei MH et al (2020) Shear thickening fluid based on silica with neodymium oxide nanoparticles. Bull Mater Sci 43(1):132
22. Wei RB, Dong B, Sun ZW et al (2021) Characterization of the rheological behaviors and mechanical properties of fabrics impregnated by different shear thickening fluids at changing temperatures. Smart Mater Struct 30:085009
23. Li S, Wang J, Cai W et al (2016) Effect of acid and temperature on the discontinuous shear thickening phenomenon of silica nanoparticle suspensions. Chem Phys Lett 658:210–214
24. Liu XQ, Bao RY, Wu XJ et al (2015) Temperature induced gelation transition of a fumed silica/PEG shear thickening fluid. RSC Adv 5(24):18367–18374
25. Yu M, Qiao XY, Dong XJ et al (2018) Shear thickening effect of the suspensions of silica nanoparticles in PEG with different particle size, concentration, and shear. Colloid Polym Sci 296(7):1119–1126
26. Shahbaz SR, Berkalp OB (2020) Effect of MWCNTs addition, on the mechanical behaviour of FRP composites, by reinforcement grafting and matrix modification. J Ind Text 50(2):205–223
27. Wei MH, Lv YR, Sun L et al (2020) Rheological properties of multi-walled carbon nanotubes/silica shear thickening fluid suspensions. Colloid Polym Sci 298(3):243–250
28. Gurgen S (2019) Tuning the rheology of nano-sized silica suspensions with silicon nitride particles. J Nano Res 56:63–70
29. Liu XG, Li Y, Xue WD et al (2018) Shear-thickening behavior of Fe-ZSM5 zeolite slurry and its removal with alumina/boehmites. Int J Miner Metall Mater 25(6):682–688
30. Hoffman RL (1982) Discontinuous and dilatant viscosity behavior in concentrated suspensions III. Necessary conditions for their occurrence in viscometric flows. Adv Colloid Interface Sci 17(1):161–184
31. Hoffman RL (1998) Explanations for the cause of shear thickening in concentrated colloidal suspensions. J Rheol 42(1):111–123
32. Wagner NJ, Brady JF (2009) Shear thickening in colloidal dispersions. Phys Today 62(10):27–32
33. Egres RG, Wagner NJ (2005) The rheology and microstructure of acicular precipitated calcium carbonate colloidal suspensions through the shear thickening transition. J Rheol 49(3):719–746
34. Olsson P, Teitel S (2007) Critical scaling of shear viscosity at the jamming transition. Phys Rev Lett 99(17):178001
35. Crawford NC, Williams SKR, Boldridge D et al (2013) Liberatore, Shear-induced structures and thickening in fumed silica slurries. Langmuir 29(42):12915–12923

36. Crawford NC, Williams SKR, Boldridge D et al (2013) Shear thickening and defect formation of fumed silica CMP slurries. Colloids Surf A 436:87–96

37. Galindo-Rosales FJ, Rubio-Hernandez FJ, Sevilla A (2011) An apparent viscosity function for shear thickening fluids. J Non-newton Fluid Mech 166(5–6):321–325

38. Zhang XZ, Li WH, Gong XL (2008) Study on magnetorheological shear thickening fluid. Smart Mater Struct 17:015051

39. Sokolovski V, Tian TF, Ding J et al (2020) Fabrication and characterisation of magnetorheological shear thickening fluids. Front Mater 7:595100

40. Yang J, Sun SS, Li WH et al (2015) Development of a linear damper working with magnetorheological shear thickening fluids. J Intell Mater Syst Struct 26(14):1811–1817

41. Liu B, Du CB, Deng HX et al (2022) Mechanical properties of magneto-sensitive shear thickening fluid absorber and application potential in a vehicle. Compos Part A Appl Sci Manuf 154:106782

42. Jolly MR, Carlson JD, Muoz BC (1996) A model of the behaviour of magnetorheological materials. Smart Mater Struct 5(5):607–614